In-Well and Barrier Coupling Pump of Semiconductor Disk Laser

Jian Feng, Bo Meng, *Senior Member, IEEE*, Cunzhu Tong, Andreas Popp, Berthold Schmidt, *Member, IEEE*, Lijie Wang, Huanyu Lu, Yanjing Wang, Xin Zhang, and Lijun Wang

***Abstract*—We report an in-well and barrier coupling pump scheme of semiconductor disk laser (SDL). An in-well-absorbed (940 nm) and a barrier-absorbed (808 nm) pump source were used to measure laser output characteristics. The output power of the coupling pump can be significantly improved compared to the in-well pump only scheme under similar thermal load conditions. The power scaling of the coupling pump SDL is caused by the interaction dynamics of the photoexcited carrier between quantum-well and barrier. The results are discussed with a rate equation model that considers the injected into the quantum-well carrier and the barrier carrier in the active region.**

***Index Terms*—Vertical-external-cavity surface-emitting laser, semiconductor disk laser, optical pumping, quantum well.**

I. Introduction

VERTICAL-external-cavity surface-emitting lasers (VECSELs), also called semiconductor thin disk lasers (SDLs), incorporate many attractive features of both semiconductor lasers and solid-state lasers. Owing to the wavelength flexibility obtained by properly designing the gain region and quantum well (QWs), SDLs have demonstrated the continuous wave (CW) and pulsed operation with wavelength spanning from UV to mid-IR via the fundamental wavelength and frequency mixing methods [1], [2], [3], [4], [5]. For the purpose of high power, reduced self-heating and enhanced heat-dissipating ability were expected. Hence, two kinds of pump approaches were developed. The conventional one is barrier pump with a pump wavelength shorter than the absorption edge of the barrier to ensure that the pump light is absorbed by the barrier/spacer regions between the QWs [6], [7]. The quantum defect, defined as the energy difference between pump- and lasing energy, typically is ∼20% in near-IR devices, and ∼50% in mid-IR devices [8], [9]. Such a large quantum defect aggravated the heat generation in SDL. The other pump approach is in-well pump [9], [10], in which the barrier/spacer regions are transparent for the pump light and absorption only occurs in the QW region. It has been applied so far to GaN-based SDL emitting at blue-violet wavelength [11], [12], [13], GaAs-based SDL emitting at red [14], [15], and near-IR [9], [10], GaSb-based SDL emitting at around 2 μm [8], [16], [17].

For in-well pumping, the main issue is the thin QWs lead to the low absorption of pump light. To enhance the absorption, the multi-pass pump scheme and the epitaxial structure with resonant wavelengths of both lasing and pump source are employed in the SDLs [9], [15]. The decrease in slope efficiency with a nonlinear increase in the threshold power density when the pump spot size was increased [18] limits the in-well pump scheme to operate with high power. These factors make it difficult for in-well pumping to reach the power level of barrier pumping although it has higher quantum efficiency, and the increased system complexity also damaged the original advantages. Obviously, the dynamics of photoexcited carriers in QWs play an important role in the performance of in-well pumped SDL, which includes the generation, relaxation, escaping, and radiative recombination process of carriers in QWs and determined the threshold, power, and efficiency of SDL. More carriers were expected to be confined in the QW to involving in the process of forming laser output instead of escaping from QW. The carrier escape process may be inhibited by barrier pump photoexcited carriers in the QW barrier. In this way, the output performance under large pump spots of the in-well pumping SDL may be improved.

In this paper, we proposed an in-well and barrier coupling pump to improve the performance of SDL unitizing the dynamics of photoexcited carriers in QWs. Based on a structure that was originally designed for conventional barrier pumping, an in-well-absorbed (940 nm) and a barrier-absorbed (808 nm) continuous-wave pump source were used to measure laser output characteristics. We studied the output power scaling and lasing threshold as a function of the additional incident laser power (808 nm & 940 nm). The carrier dynamics in barrier and QW

Manuscript received 9 July 2022; revised 4 September 2022; accepted 19 September 2022. Date of publication 22 September 2022; date of current version 3 October 2022. This work was supported in part by the National Natural Science Foundation of China under Grants 61790584 and 62025506, in part by TRUMPF Company, and in part by K.C.Wong Education Foundation. *(Corresponding author: Cunzhu Tong.)*

Jian Feng is with the State Key Laboratory of Luminescence and Application, Changchun Institute of Optics, Fine Mechanics and Physics, Chinese Academy of Sciences, Changchun 130033, China, and also with the Center of Materials Science and Optoelectronics Engineering, University of Chinese Academy of Sciences, Beijing 100049, China (e-mail: fengjian12453@163.com).

Bo Meng, Cunzhu Tong, Lijie Wang, Huanyu Lu, Yanjing Wang, Xin Zhang, and Lijun Wang are with the State Key Laboratory of Luminescence and Application, Changchun Institute of Optics, Fine Mechanics and Physics, Chinese Academy of Sciences, Changchun 130033, China (e-mail: mengbo@ciomp.ac.cn; tongcz@ciomp.ac.cn; wanglijie@ciomp.ac.cn; luhuanyu@ciomp.ac.cn; wangyanjing@ciomp.ac.cn; zhang315xin@ciomp.ac.cn; wanglj@ciomp.ac.cn).

Andreas Popp and Berthold Schmidt are with the TRUMPF GmbH+Co.KG, 71254 Ditzingen, Germany (e-mail: andreas.popp@de.trumpf.com; berthold.schmidtwanglj@ciomp.ac.cn@trumpf.com).

Digital Object Identifier 10.1109/JPHOT.2022.3208738

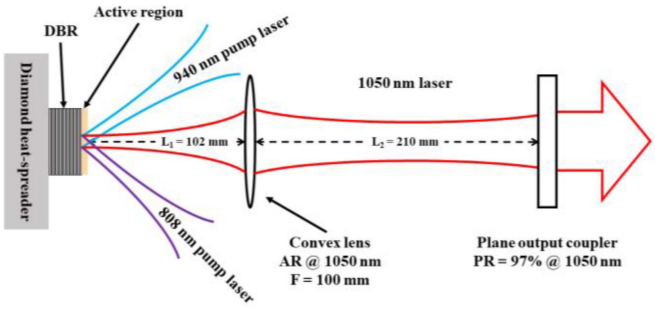

Fig. 1. Schematic diagram of the experiment setup.

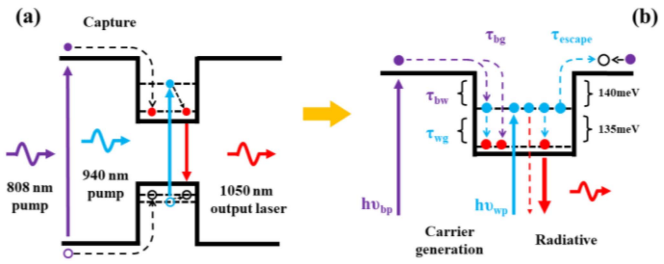

Fig. 2. (a) Schematic diagram of in-well and barrier coupling pump SDL laser band-edge profile. The purple arrows indicate an 808 nm pump photon is absorbed in the barriers surrounding the QW. The blue arrows indicate a 940 nm pump photon is absorbed in the QW. After relaxation to the ground state, all the carriers in the QW recombine into 1050 nm laser pho-ton (red arrows). (b) Schematic sketch of the in-well and barrier coupling pump photoexcited carrier relaxation pathways in a confined sub-band.

and the relaxation pathways are considered. The lasing spectrum reflecting the transport mechanism and temperature characteristics of the carriers was investigated.

II. Experimental Setup

The investigated active medium of the SDL chip was grown by metal-organic vapor phase epitaxy (MOVPE) on a GaAs substrate in reverse order. The active region consists of ten inverted 8 nm InGaAs QWs, equally spaced by GaAsP barrier layers with optimized anti-node positions of the standing wave in the optical cavity (a resonant periodic gain placement) to ensure a low threshold and homogeneous gain. 20 pairs of AlAs/GaAs layer form the distributed Bragg reflector (DBR), which has a reflectivity higher than 99.9% at 1050 nm. The gain chip was cut into 3 mm $\times$ 3 mm pieces. In order to minimize the effect of waste heat generated by pump laser, thermal management of the gain medium was achieved by bonding to a pre-metalized diamond heat spreader via solid-liquid-interdiffusion bonding [19]. After the packaging step, the semiconductor substrate is removed by selective wet etching. No anti-reflective coating is applied to fully exploit the resonant gain enhancement by the sub-cavity mode [20], [21], [22]. The sample was further mounted to a copper heatsink which was cooled by a Peltier element.

Fig. 1 shows the laser setup used in the experiments. The laser cavity was formed by the SDL chip's DBR as one end mirror and a plane output coupler on the other end. In order to take into account the transmittance of the barrier pumping output coupling mirror, we choose the conventional 3% instead of 0.8% which is more suitable for in-well pumping [9]. A plano-convex lens was set in the cavity to cooperate with the flat output coupler to form a stable resonant cavity. The cavity length $L_1 = 102$ mm and $L_2 = 210$ mm. The diameter of the mode size on the gain chip is $\sim$127 μm so that the laser can operate in multi-mode with high output power.

A barrier-absorbed 808 nm wavelength pump source and a 940 nm wavelength in-well-absorbed pump source were selected for the verification experiment. For in-well pumping, the shorter wavelength of the pump light, the larger photon energy, and the greater the intrinsic absorption coefficient of QW to the pump light. However, large pump photon energy will also lead to large quantum defects, an obvious thermal effect, and a weaker confinement effect of QW on excited carriers [9], [23]. Due to the pump photon being absorbed in the QW and creating an electron-hole pair, the conduction band and valence band have the same number of electrons and holes. Here we only consider the electron relaxation process. Therefore, we chose a 940 nm laser as the in-well pump source, which electron energy level is about half of the QW conduction band depth. Both beams of the pump light were imaged at the same point onto the SDL chip surface. At a near 30° angle of incidence, a slight angle difference was introduced to prevent the two pump beams from reflecting into each other. The main difference between the pump laser was the pump-spot size. The barrier-absorbed 808 nm pump laser was focused into a spot with a diameter of $\sim$400 μm and the in-well-absorbed 940 nm pump laser was $\sim$300 μm. This is so that the in-well pumping area can be completely covered by the barrier pumping area.

For the SDL optimized for high power operation, the heat-spreader was measured in a temperature range of 10 $\pm$ 1 °C. Because the epitaxial structure is designed for conventional barrier pumping, the DBR is optimized only for the emission wavelength. The reflectance of the DBR around 940 nm is only $\sim$60%, and any transmission of the remaining pump light through the DBR below the gain region would lead to further heating of the structure [10]. The absorption efficiency of the 940 nm pump laser by QW η_{wa} is $\sim$20%. The reflectance of the DBR around 808 nm is $\sim$40%, and the absorption efficiency of the 808 nm pump laser by active region η_{ba} is $\sim$87%.

III. Theoretical Background

For in-well pumping, the barrier/spacer regions are transparent to the pump wavelength and the absorption of pump light only occurs in the QW region. We use a simple model to discuss the dynamics of photo-excited carriers in QW. As shown in Fig. 2, three relaxation pathways of the in-well excited states were considered.

The carrier loss rate for QW photoexcited carrier density N_w at a given con-fined sub-band can be expressed as

$$\frac{N_w}{\tau} = N_w \left(\frac{1}{\tau_{escape}} + \frac{1}{\tau_{rad}} + \frac{1}{\tau_{nonrad}} \right) \tag{1}$$

where τ_{escape}, τ_{rad}, and τ_{nonrad} are the escape, radiative recombination, and non-radiative relaxation times, respectively. When in-well pumped SDL operates in continuous wave (CW) mode, the carriers were injected directly into the QW and relaxed to

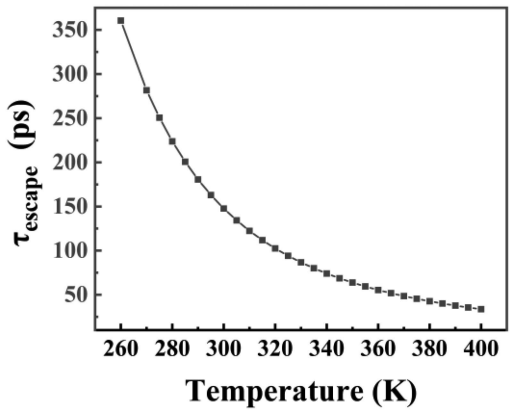

Fig. 3. Temperature dependence of the thermal escape time τ_{escape} of the SDL.

TABLE I
LASER AND MATERIAL PARAMETERS USED IN THE CALCULATION

Symbol	Value	Units	Symbol	Value	Units
R_1	0.999	-	A	$1*10^{7}$	s^{-1}
R_2	0.97	-	B	$1*10^{-10}$	$cm^3\ s^{-1}$
T_{loss}	0.965	-	C	$6*10^{-30}$	$cm^6\ s^{-1}$
g_0	2200	cm^{-1}	Γ	2	-
N_0	$1.7*10^{18}$	cm^{-3}	A_{mode}	$\pi(63.5)^2$	μm^2
τ_b	2	ns	A_b	$\pi(200)^2$	μm^2
τ_w	1	ns	A_w	$\pi(150)^2$	μm^2
τ_{bg}	20	ps	L_b	1.6	μm
τ_{wg}	4	ps	L_w	8	nm
τ_{bw}	16	ps	n_w	10	-

the ground state of QW through non-radiative relaxation. Then carriers located at the ground state recombined to generate the photons. This process dominates the entire carrier dynamics injected into the QW. The carrier escape and radiation recombination processes are relatively weak and negligible.

However, when the pump power increases and the QW temperature rises, the carrier escape process cannot be ignored. Especially in the SDL, a number of 8 to 18 QWs are used in the gain structure for high modal gain. The amount of escaped carriers due to the thermal effect becomes enriched at high temperatures and high-power operation. In the undoped SDL epitaxial structure, the rate of carriers' escape from the QW can be expressed by [24]:

$$\frac{N_w}{\tau_{escape}} \approx \frac{N_w}{\tau_{th}} = \frac{N_w}{L_w}\sqrt{\frac{kT}{2\pi m_w}}\exp\left(\frac{-\Delta E}{kT}\right) \tag{2}$$

where τ_{th} is the thermal escape time, $L_w = 8$ nm is the QW width, $m_\omega = 0.057m_0$ is the effective mass of carrier in the QW, and ΔE is the energy barrier height of QW. L_w is fixed for a single QW. ΔE and m_ω are also determined at a fixed in-well pump wavelength.

The escape rate of photoexcited carriers in the QW is mainly determined by the QW temperature T and the injected carrier density N_w. Based on the parameters used in our experimental conditions, we can calculate the carrier escape time τ_{escape} for in-well pumping, the result is shown in Fig. 3. The τ_{escape} decreases with the increase of temperature and will be less than 100 ps above 320 K. It is close in value of τ_{bg} ($\sim$20 ps), the carrier capture time from the barrier into the ground states of QW [25]. Therefore, the carrier thermal escape effect may be one of the reasons why the pump spot size and pump power cannot be increased in the in-well pumping, thereby limiting its performance improvement.

In the QW, recombination and escape are two competing processes whereby one increases at the expense of the other one [26], [27]. For the carrier escape process, the barrier energy state that would otherwise be occupied by the escaped carriers will be occupied by the carriers excited by the barrier pump light, and the competition between them will inhibit the escape of the carriers. On the other hand, the carriers that have escaped the QW are counted in N_b and will be re-captured by the QW. With the increase of N_b, the N_b/τ_{bg} rate will also increase. Both above processes will increase the number of carriers injected into the QW ground state N_g, and the non-radiative relaxation of carriers is reduced. In terms of laser performance, the threshold of coupling pump power will be reduced and the output power will be improved.

Assuming the carriers injected into the QW can directly relax to the QW ground state through non-radiative relaxation and participate in the radiation recombination process of the ground state, $\tau_{nonrad} = \tau_{wg}$, as shown in Fig. 2(b). The rate equations for in-well and barrier coupling pump SDL can be written as

$$\frac{dN_b}{dt} = \frac{\eta_{bp}P_{bp}}{h\nu_{bp}V_b} + \frac{N_wV_w}{\tau_{escape}V_b} - \frac{N_b}{\tau_{bw}} - \frac{N_b}{\tau_{bg}} - \frac{N_b}{\tau_b} \tag{3}$$

$$\frac{dN_w}{dt} = \frac{\eta_{wp}P_{wp}}{h\nu_{wp}V_w} + \frac{N_bV_b}{\tau_{bw}V_w} - \frac{N_w}{\tau_{escape}} - \frac{N_w}{\tau_{wg}} - \frac{N_w}{\tau_w} \tag{4}$$

$$\frac{dN_g}{dt} = \frac{N_bV_b}{\tau_{bg}V_w} + \frac{N_w}{\tau_{wg}} - \frac{N_g}{\tau_g} - v_ggS \tag{5}$$

$$\frac{dS}{dt} = \Gamma v_ggS - \frac{S}{\tau_p} + \Gamma\beta_{sp}R_{sp} \tag{6}$$

where g is the optical gain, S is the photon density of laser, Γ is the optical confinement factor, v_g is the group velocity of the photon, τ_p is the photon lifetime, β_sp is the spontaneous emission factor, R_{sp} is the spontaneous emission rate, τ_b and τ_w are the carrier recombination lifetime in the barrier state and in-well bound state, τ_{bw} is the carrier capture time by the in-well bound states of the QW from the barrier states, τ_{bg} and τ_{wg} are the approximate value of the carrier capture time by the ground states of the QW from the barrier states and the in-well bound states, respectively. The laser and material parameters for the calculation are summarized in Table I [6], [25].

When we study the threshold characteristics, the pump power injection efficiency of barrier and in-well pumping are $\eta_{bp} = \eta_{ba}\ \alpha_{bp}\ (A_{mode}/A_b)$ and $\eta_{wp} = \eta_{wa}\ (A_{mode}/A_w)$ respectively. $V_b = L_bA_b$ and $V_w = n_wL_wA_w$ are the volumes of the barrier and the QW layers. A_{mode}, A_b, and A_w are the area of laser-mode, barrier pump, and in-well pump. n_w, L_w, and L_b

are the number of QW and the thickness of the QW, and the barrier layers. The carrier recombination lifetime of the ground state of the QW $\tau_g(N_g) = 1/(A+BN_g+CN_g^2)$, where A, B, and C are the monomolecular, bimolecular, and Auger recombination coefficients. The thresh-old carrier density $N_{th} = N_0(R_1R_2T_{loss})^{-1/(2\Gamma g0nwLw)}$ [6], where R_1 and R_2 are the DBR and the output coupler mirror reflectivity, T_{loss} is the round-trip loss transmission factor, g_0 is the material-gain parameter, N_0 is the transparency carrier density. Except for the thermal escape carrier, other temperature variables are approximate to the $N_{th} \propto exp(T/T_0)$ and the characteristic temperature $T_0 \approx 100$K. The laser and material parameters for the calculation are summarized in Table I. Through the rate equation (3)–(6), we can calculate the relationship between the threshold of pump power P_{bp} and P_{wp} in the coupling pump process, as shown in Fig. 3(b). In the coupling pumping, the threshold for the P_{bp} and the P_{wp} decrease as one of them increases. While the overall threshold rises with the increasing temperature.

The laser output power P_{out} can be calculated by the differential efficiency η_d. For the in-well/barrier pumping, $\eta_{(w/b)d} = \eta_{out}\eta_{(w/b)q}\eta_{(w/b)abs}$. The output efficiency is determined by the external cavity parameters, $\eta_{out} = ln(R_2)/ln(R_1R_2T_{loss})$, and the quantum efficiency is determined by the pump wavelength, $\eta_{(w/b)q} = \lambda_{(w/b)p}/\lambda_{laser}$. Here we can get the differential efficiency $\eta_{wd} = 0.0813$ and $\eta_{bd} = 0.304$. The low absorption efficiency of the in-well pump is the main reason for the low η_{wd}. Compared with the in-well pump, the absorption efficiency and temperature characteristics of the barrier pump are more linear, so when calculating the P_{out} of the coupling pump, we set the CW P_{bp} to a fixed value. The P_{out} can be divided into the in-well pump and barrier pump contribution, $P_{out} = P_{wout} + P_{bout}$. The temperature of the heat sink set by the controller in the experiment is approximately 280 K. The output power contributed by the barrier pump can be described as $P_{bout} = \eta_{bd}\,(P_{bp} - P_{bth})$, only when P_{bp} is greater than the threshold of barrier pump P_{bpth}. The initial temperature and threshold of the in-well pumped part P_{wout} will vary with the injection of the P_{bp}. The temperature rise caused by the injection of P_{bp} is calculated according to thermal impedance $R_{th} = 1.25$ K/W, as shown in our previous work [19]. The P_{wout} can be approximately given by $P_{wout} = \eta_{wd}\,(P_{wp} - P_{wpth}) + \eta_{bd}\,(P_{bp} - P_{bpth})\,(P_{wp}/(P_{bp}+P_{wp}))$, and thus get P_{out} versus P_{wp} at different P_{bp} and temperatures. The result is shown in Fig. 4(b). In addition to increasing the P_{out}, the injection of a barrier pump laser in the coupling pump will also introduce more serious quantum defects and thermal effects. The thermal rollover effect is not considered in the calculation results.

IV. Experimental Results and Discussion

At first, the operation of the SDLs was pumped at in-well-absorbed 940 nm wave-length, the output power versus incident pump power curves was shown in Fig. 5(a). With 940 nm pumping only (black line), we achieve a maximum output power of 2.11W. This output power level is comparable to previous experimental and theoretical reports [9], [15], [23]. At the end of the power curve, the slope of the curve tends to remain constant.

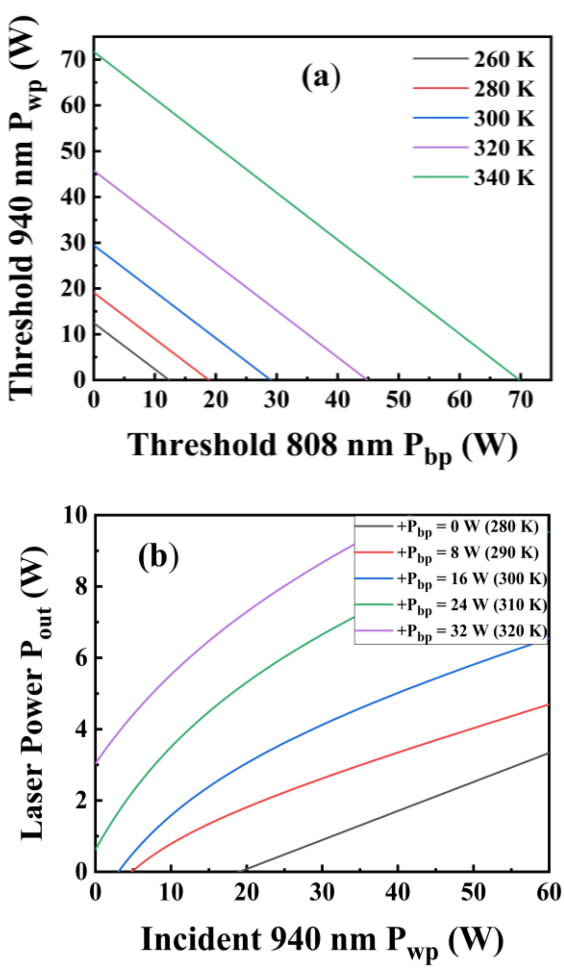

Fig. 4. The simulated threshold of in-well pump power P_{wp} and barrier pump power P_{bp} in the coupling pump system at different temperatures. (b) The simulated output laser power of the coupling pump P_{out} at different fixed P_{bp} and temperatures.

Meanwhile, the carrier escape rate increase until it is balanced with the radiative and nonradiative rate as given by (1).

In the coupling pump, we first consider the in-well pump leading case, a barrier-absorbed 808 nm pump laser with fixed power as an additional injected pump source in the in-well pump process. For the resonator configuration of this experiment, if only an 808 nm pump laser was injected the threshold of P_{bp} is 16.8 W. With the P_{bp} level upping from zero to 16.8 W, the threshold of P_{wp} has significantly decreased, and the slope and the maximum output power P_{out} have significantly increased. The maximum P_{out} increased from 2.11 W to 5 W, as shown in Fig. 5(b). As given by (5), the carrier density N_g contributed mainly by N_w/τ_{wg} from the in-well pumping and $N_bV_b/\tau_{bg}V_w$ from the barrier pumping. For the coupling pump, the additional injection N_b increases both N_w/τ_{wg} and $N_bV_b/\tau_{bg}V_w$, as given by (3)–(5). The carriers escaping from the QW will make N_b larger than that excited by the barrier pump laser alone. For in-well pumping, the increase in N_b and $N_bV_b/\tau_{bg}V_w$ makes less N_w/τ_{wg} required for N_g to reach the threshold condition. The suppressed carrier escape process and a small amount of $N_bV_b/\tau_{bw}V_w$ will increase the N_w/τ_{wg}. The above reasons together lead to the increase of N_g and P_{out}.

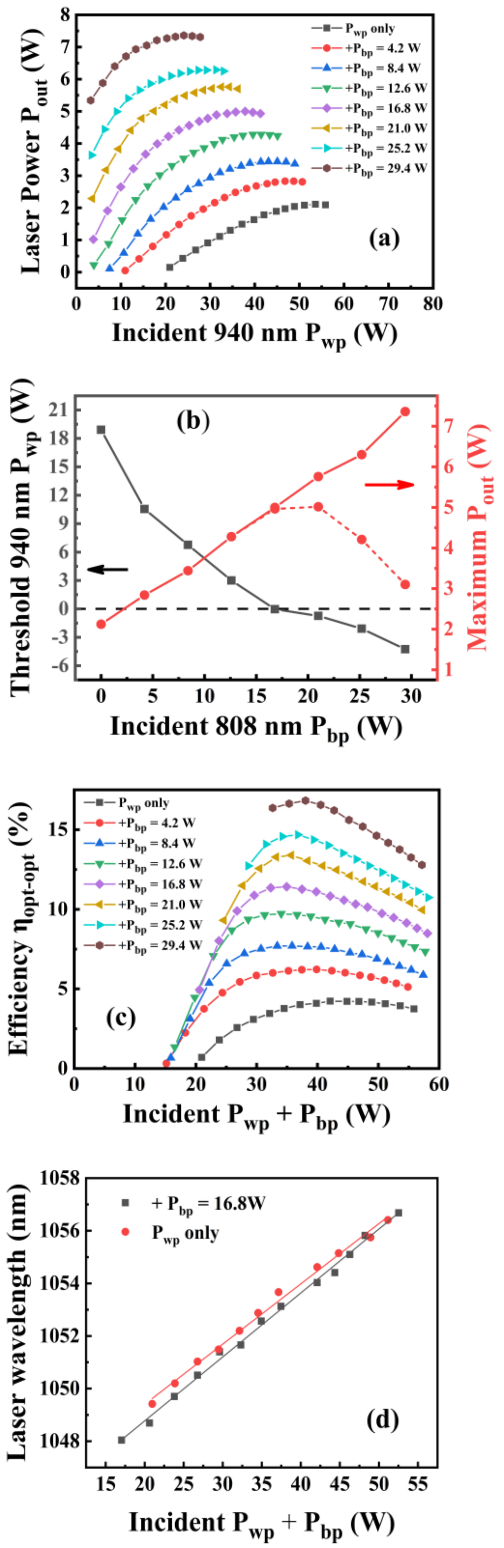

Fig. 5. (a) Pump-output power characteristics of the SDL for 940 nm P_{wp} with varying 808 nm P_{bp}. (b) Comparison of the threshold P_{wp} (left vertical axis) and maximum P_{out} (right vertical axis) as a function of different incident P_{bp}. The negative part of the threshold is the laser output power at the 808 nm pump condition. The red dash line of the maximum P_{out} is the actual total value minus the negative value. (c) The optical-optical efficiency $\eta_{opt\text{-}opt}$ versus the total incident pump power $P_{wp} + P_{bp}$ with varying P_{bp} as in (a). (d) The peak emission wavelength of the coupling pump SDL at different pump power in the 940 nm in-well pump leading case.

The overall optical-optical efficiency $\eta_{opt\text{-}opt}$ has been significantly improved, as shown in Fig. 5(c). That means under the same total pump power $P_{wp} + P_{bp}$, more carriers relax to the ground state of the QW and involve in radiative recombination than using the only in-well pump. The intrinsic efficiency is improved [9]. Fig. 5(d) shows the peak emission wavelength of the output laser pumped by P_{wp} only and the coupling pump with an additional $P_{bp} = 16.8$ W, corresponding to the black and purple curves in Fig. 5(a) and (c). When the total pump power is close in value, the output power of the coupling pump is 5 W greater than that of the in-well pump is only 2.11 W, but the difference between the peak emission wavelength is only about 0.4 nm. This means that the additional P_{bp} injected below the threshold in the coupling pump does not produce too much additional heat, but improves both $\eta_{opt\text{-}opt}$ and P_{out}.

With the incident 808 nm P_{bp} raising from 16.8 W to 29.4 W, the maximum P_{out} is also increased. Under this condition, P_{bp} is already higher than its own threshold, as shown by the negative part of the black line in Fig. 5(b). For the coupling pump, the contribution of in-well pumping to output power decreases, and the pumping process gradually changes to barrier pump dominant, as shown by the red dash line in Fig. 5(b). With the further increase of the P_{bp} level, the overall optical-optical efficiency $\eta_{opt\text{-}opt}$ drops rapidly after reaching the peak, as shown in Fig. 5(c). Because the heat generated by the quantum defect of $N_b V_b / \tau_{bg} V_w$ increases accordingly with the P_{bp}. Meanwhile, as the temperature of the QW increases, the carrier escape rate also increases. An increase in the number of carriers escaping from the QW and subsequently re-captured by the ground state of the QW will generate more heat. Therefore, a higher P_{bp} above the threshold will compete and displace the in-well pumping, and bring about more severe thermal effects. For in-well pumping, an additional barrier pump source with power below the threshold will effectively suppress the carrier escape effect and improve the laser output performance.

In the relative case of the 808 nm barrier pump leading coupling pump, a 940 nm in-well-absorbed pump laser as an additional pump source was injected into the active region. The P_{out} versus incident 808 nm P_{bp} is shown in Fig. 6(a). With 808 nm pumping only (black line), we can achieve a maximum $P_{out} = 12.19$ W. When the P_{bp} is less than 40 W, the additional injected P_{wp} enables a lower threshold and a higher output power. Because the carriers excited by P_{wp} and relaxed through N_w / τ_{wg} directly increase the N_g, then the N_g can achieve threshold carrier density by capturing fewer barrier carriers. When the P_{bp} is more than 40 W, the maximum P_{out} decrease is mainly caused by the thermal effect. The high temperature brought by high P_{bp} makes the device thermal rollover. Under this condition, the carrier escape rate of N_w will be too large to be ignored and the escaped carriers re-captured by the ground state of the QW will generate more heat. The total amount of heat dissipation capacity is constant, so the additional injected P_{wp} will advance the rollover point. The same result is also shown in Fig. 6(b).

Similar optical-optical efficiency results induced by thermal effects are shown in Fig. 6(c). Under the same total pump power

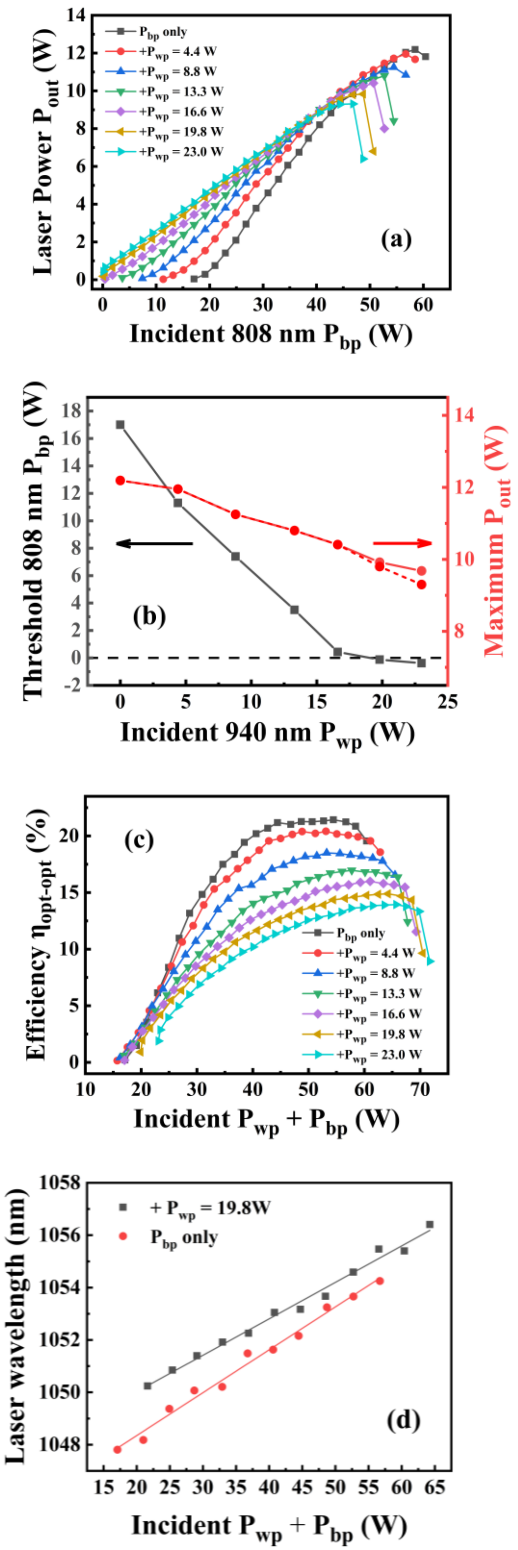

Fig. 6. (a) Pump-output power characteristics of the SDL for 808 nm P_{bp} with varying 940 nm P_{wp}. (b) Comparison of the threshold P_{bp} (left vertical axis) and maximum P_{out} (right vertical axis) as a function of different incident P_{wp}. The negative part of the threshold is the laser output power at the 940 nm pump condition. The red dash line of the maximum P_{out} is the actual total value minus the negative value. (c) The optical-optical efficiency $\eta_{opt\text{-}opt}$ versus the total incident pump power P_{wp}+P_{bp} with varying P_{wp} as in (a). (d) The peak emission wavelength of the coupling pump SDL at different pump power in the 808 nm barrier pump leading case.

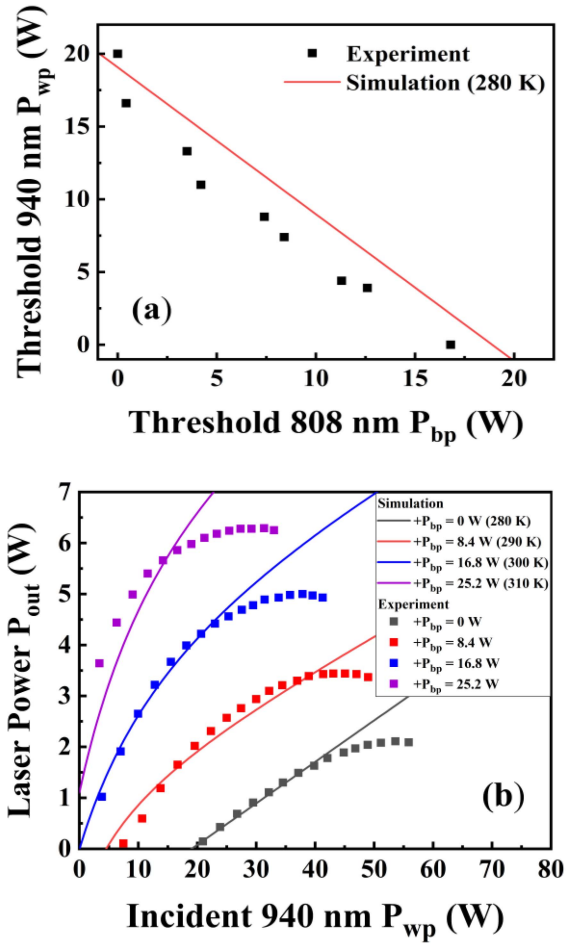

Fig. 7. (a) The simulated and experimental threshold of in-well pump power P_{wp} and barrier pump power P_{bp} in the coupling pump system at 280 K. (b) The simulated and experimental output laser power of the coupling pump P_{out} at different fixed P_{bp} and temperatures.

$P_{wp} + P_{bp}$, in addition to the thermal effect of carrier relaxation, the decrease of efficiency $\eta_{opt\text{-}opt}$ is also due to the additional heat generated by the low absorption efficiency of P_{wp}. Fig. 6(d) shows the peak emission wavelength of the output laser pumped by P_{bp} only and the coupling pump with an additional $P_{wp} =$ 19.8 W, corresponding to the black and brown curves in Fig. 6(a) and (c). The peak emission wavelength of the coupling pump is overall longer than the P_{bp} pump only. Their average difference is greater than 1.2 nm, especially at low pump power. This indicates that the heat load brought by the P_{wp} injection is greater than the gain contribution in the barrier pump leading coupling pump. The thermal effect reduces the achievable output power.

We compared the threshold results of the concept of coupling pump (red line in Fig. 4(a)) with the experimental value at 280 K (positive part of black curves in Figs. 5(b) and 6(b)). The results are shown in Fig. 7(a). The threshold variation trend of coupled pumping is basically in line with the predictions of our theoretical simulations. The simulated and experimental P_{out} of the coupling pump at different fixed P_{bp} and temperatures are shown in Fig. 7(b). The experimental values are the same as the corresponding curves given in Fig. 5(a). According to the actual P_{bp} values used in the experiments, we fine-tune the simulated

values in Fig. 4(b). As explained above, the relative error of P_{out} is caused by the carrier thermal effect and rollover. Overall, the measurement is a demonstration of the applicability of the coupling pump rate equations for the output characterization.

V. Conclusion

In summary, we have presented an in-well and barrier coupling pump scheme of semiconductor disk laser. We have investigated the carrier dynamics characteristics of the coupling pump and give a reliable rate equation model. As a mechanism to limit the improvement of the output performance of in-well pump SDL, the carrier thermal escape effect will be significantly improved by the coupling pump scheme. In the in-well pump leading coupling pump case, the optical-optical efficiency and output power can be significantly improved by introducing a barrier absorption pump source under a similar thermal load. The threshold of the in-well/barrier pump can be significantly reduced by introducing a barrier/in-well absorption pump source. Although the improvement brought by the coupling pump is obvious, it is still a difficult task and the overall optical efficiency is relatively low, primarily due to the low absorption of the in-well pump source. We believe that combining the coupling pump approach with existing methods for improving the absorption efficiency of the in-well pump laser, such as resonant pumping and multi-pass pumping [9], [15], [28], can achieve more efficient pumping and higher output power simultaneously. Furthermore, for some visible and mid-IR wavelength SDL devices which have no commercial high power pump source with a suitable wavelength, our approach can also provide a potential solution.

References

[1] M. Guina, A. Rantamaki, and A. Harkonen, "Optically pumped VECSELs: Review of technology and progress," *J. Phys. D Appl. Phys.*, vol. 50, no. 38, Sep. 2017, Art. no. 383001, doi: 10.1088/1361-6463/aa7bfd.

[2] S. Shu et al., "Progress of optically pumped GaSb based semiconductor disk laser," *Opto-Electron. Adv.*, vol. 1, no. 2, 2018, Art. no. 170003, doi: 10.29026/oea.2018.170003.

[3] B. W. Tilma et al., "Recent advances in ultrafast semiconductor disk lasers," *Light: Sci. Appl.*, vol. 4, no. 7, pp. e310–e310, 2015, doi: 10.1038/lsa.2015.83.

[4] S. Calvez, J. E. Hastie, M. Guina, O. G. Okhotnikov, and M. D. Dawson, "Semiconductor disk lasers for the generation of visible and ultraviolet radiation," *Laser Photon. Rev.*, vol. 3, no. 5, pp. 407–434, 2009, doi: 10.1002/lpor.200810042.

[5] B. Heinen et al., "106 W continuous-wave output power from vertical-external-cavity surface-emitting laser," *Electron. Lett.*, vol. 48, no. 9, pp. 516–517, 2012, doi: 10.1049/el.2012.0531.

[6] M. Kuznetsov, F. Hakimi, R. Sprague, and A. Mooradian, "Design and characteristics of high-power(>0.5W CW) diode pumped vertical external cavity surface emitting semiconductor lasers with circular TEM00 beams," *IEEE J. Sel. Topics Quantum Electron.*, vol. 5, no. 3, pp. 561–573, May/Jun. 1999, doi: 10.1109/2944.788419.

[7] T.-L. Wang et al., "Quantum design strategy pushes high-power vertical-external-cavity surface-emitting lasers beyond 100 W," *Laser Photon. Rev.*, vol. 6, no. 5, pp. L12–L14, 2012, doi: 10.1002/lpor.201200034.

[8] N. Schulz et al., "Resonant optical in-well pumping of an (AlGaIn)(AsSb)-based vertical-external-cavity surface-emitting laser emitting at 2.35μm," *Appl. Phys. Lett.*, vol. 91, no. 9, 2007, Art. no. 1063, doi: 10.1063/1.2773970.

[9] S. S. Beyertt et al., "Optical in-well pumping of a semiconductor disk laser with high optical efficiency," *IEEE J. Quantum Electron.*, vol. 41, no. 12, pp. 1439–1449, Dec. 2005, doi: 10.1109/Jqe.2005.858794.

[10] M. Schmid, S. Benchabane, F. Torabi-Goudarzi, R. Abram, A. I. Ferguson, and E. Riis, "Optical in-well pumping of a vertical-external-cavity surface-emitting laser," *Appl. Phys. Lett.*, vol. 84, no. 24, pp. 4860–4862, 2004, doi: 10.1063/1.1760887.

[11] T. Wunderer et al., "In-well pumping of InGaN/GaN vertical-external-cavity surface-emitting lasers," *Appl. Phys. Lett.*, vol. 99, no. 20, 2011, Art. no. 201109, doi: 10.1063/1.3663575.

[12] R. Debusmann, U. Brauch, V. Hoffmann, M. Weyers, and M. Kneissl, "Spacer and well pumping of InGaN vertical cavity semiconductor lasers with varying number of quantum wells," *J. Appl. Phys.*, vol. 112, no. 3, pp. 33–110, 2012, doi: 10.1063/1.4745025.

[13] K. S. Adam et al., "Concept of the CW GaN-based VECSEL," in *Proc. SPIE Conf. Vertical External Cavity Surf. Emitting Lasers (VECSELs) VIII*, vol. 10515, pp. 102–109, 2018, Art. no. 105150X, doi: 10.1117/12.2290391.

[14] C. M. N. Mateo et al., "Enhanced efficiency of AlGaInP disk laser by in-well pumping," *Opt. Exp.*, vol. 23, no. 3, pp. 2472–2486, 2015, doi: 10.1364/OE.23.002472.

[15] C. Mateo et al., "2.5W continuous wave output at 665nm from a multipass and quantum-well-pumped AlGaInP vertical-external-cavity surface-emitting laser," *Opt. Lett.*, vol. 41, no. 6, pp. 1245–1248, 2016, doi: 10.1364/OL.41.001245.

[16] J. Wagner et al., "Barrier- and in-well pumped GaSb-based 2.3 μm VECSELs," *Physica Status Solidi*, vol. 4, no. 5, pp. 1597–1600, 2007, doi: 10.1002/pssc.200674274.

[17] N. Schulz et al., "An improved active region concept for highly efficient GaSb-based optically in-well pumped vertical-external-cavity surface-emitting lasers," *Appl. Phys. Lett.*, vol. 93, no. 18, 2008, Art. no. 181113, doi: 10.1063/1.3013311.

[18] M. N. M. Cherry et al., "Efficiency and power scaling of in-well and multi-pass pumped AlGaInP VECSELs," in *Proc. SPIE Conf. Vertical External Cavity Surf. Emitting Lasers (VECSELs) VIII*, vol. 9734, pp. 177–183, 2016, Art. no. 973410, doi: 10.1117/12.2212162.

[19] G. Y. Hou, S. L. Shu, J. Feng, A. Popp, and L. J. Wang, "High power (>27 W) semiconductor disk laser based on pre-metalized diamond heat-spreader," *IEEE Photon. J.*, vol. 11, no. 2, Apr. 2019, Art. no. 1501908, doi: 10.1109/JPHOT.2019.2908876.

[20] J. V. Moloney, J. Hader, and S. W. Koch, "Quantum design of semiconductor active materials: Laser and amplifier applications," *Laser Photon. Rev.*, vol. 1, no. 1, pp. 24–43, 2007, doi: 10.1002/lpor.200610003.

[21] E. Kuehn, A. Thraenhardt, C. Bueckers, S. W. Koch, J. Hader, and J. V. Moloney, "Numerical study of the influence of an antireflection coating on the operating properties of vertical-external-cavity surface-emitting lasers," *J. Appl. Phys.*, vol. 106, no. 6, 2009, Art. no. 063105, doi: 10.1063/1.3224875.

[22] C. Bückers et al., "Quantum modeling of semiconductor gain materials and vertical-external-cavity surface-emitting laser systems," *Physica Status Solidi*, vol. 247, no. 4, pp. 789–808, 2010, doi: 10.1002/pssb.200945432.

[23] E. Kühn, S. W. Koch, A. Thränhardt, J. Hader, and J. V. Moloney, "Microscopic simulation of nonequilibrium features in quantum-well pumped semiconductor disk lasers," *Appl. Phys. Lett.*, vol. 96, no. 5, 2010, Art. no. 051116, doi: 10.1063/1.3294628.

[24] H. Schneider and K. Vonklitzing, "Thermionic emission and gaussian transport of holes in a GaAs/AlxGa1-xAs multiple-quantum-well structure," *Phys. Rev. B*, vol. 38, no. 9, pp. 6160–6165, Sep. 1988, doi: 10.1103/PhysRevB.38.6160.

[25] A. R. Zakharian, J. Hader, J. V. Moloney, S. W. Koch, P. Brick, and S. Lutgen, "Experimental and theoretical analysis of optically pumped semiconductor disk lasers," *Appl. Phys. Lett.*, vol. 83, no. 7, pp. 1313–1315, 2003, doi: 10.1063/1.1601672.

[26] J. Barnes, E. S. M. Tsui, K. W. J. Barnham, S. C. McFarlane, C. Button, and J. S. Roberts, "Steady state photocurrent and photoluminescence from single quantum wells as a function of temperature and bias," *J. Appl. Phys.*, vol. 81, no. 2, pp. 892–900, 1997, doi: 10.1063/1.364136.

[27] A. Alemu, J. A. H. Coaquira, and A. Freundlich, "Dependence of device performance on carrier escape sequence in multi-quantum-well p-i-n solar cells," *J. Appl. Phys.*, vol. 99, no. 8, 2006, Art. no. 084506, doi: 10.1063/1.2191433.

[28] B. Uwe et al., "Schemes for efficient QW pumping of AlGaInP disk lasers," in *Proc. SPIE Conf. Vertical External Cavity Surf. Emitting Lasers (VECSELs) VIII*, vol. 10087, pp. 9–21, 2017, Art. no. 1008703, doi: 10.1117/12.2250901.